

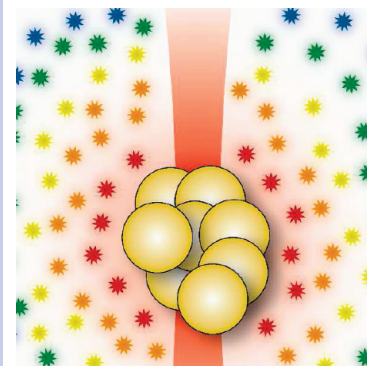
# Monitoring Photothermally Excited Nanoparticles via Multimodal Microscopy

Matthew L. Clarke, Shin Grace Chou, and Jeeseong Hwang\*

National Institute of Standards and Technology, Optical Technology Division, 100 Bureau Drive, Gaithersburg, Maryland 20899

**ABSTRACT** Generation of heat using optically excited nanoparticles can be beneficial or detrimental depending on the application. Therefore, clinically applicable studies are being pursued in an effort to identify safe practices of nanoparticle-induced hyperthermia for the treatment of cancerous tissues using optical radiation. The imaging and characterization of localized heat production resulting from optically excited nanoparticles on both cellular and tissue levels is important for determination of nanoparticle dosage and optimal conditions for the radiation. In this report, we present a multimodal imaging method to monitor the local temperature change induced by photothermally excited, biologically relevant gold nanoshell clusters on the micrometer scale using two types of temperature-sensitive fluorescent reporters: Indo-1 or semiconductor quantum dots. The photoinduced heat flux from gold nanoshells is observed to be dependent on the dynamic motion of nanoparticles in the induced thermal gradient, with phenomena such as nanoparticle focusing strongly influencing the local temperature elevation.

**SECTION** Nanoparticles and Nanostructures



Gold nanoparticles have been increasingly employed as novel tools for clinical therapies. For hyperthermia in cancer treatment, nanoparticle-based photothermal therapies have been demonstrated to selectively destroy cancerous cells using gold nanorods,<sup>1</sup> nanoshells,<sup>2</sup> and nanocages<sup>3</sup> excited by near-infrared (NIR) light. These nanoparticles can be delivered in vivo to target cancerous tissues via the blood, both nonspecifically (e.g., via the tumor leaky vasculature) or specifically using antibody targets.<sup>4</sup> After the nanoparticles accumulate to effective levels at the target site, irradiation leads to elevated local temperatures. Enhanced cell lethality has been experimentally demonstrated for the adsorption of clusters of nanoparticles to cells.<sup>5,6</sup> While models exist for the nonradiative energy transfer mechanisms and heat-flux optimization from single photothermally excited nanoparticles,<sup>7–10</sup> clinically relevant samples will include a wide distribution of nanoparticle cluster sizes not accounted for by simple models. For safe dosimetry decisions in hyperthermia applications, measurement of localized heat generation induced by NIR radiation on groups of nanoparticles is crucial.

Multimodal optical imaging combining NIR microscopy and fluorescence microscopy can fill the gap between experimental measurements of bulk systems<sup>11</sup> and single nanoparticles.<sup>12</sup> Such an integrated imaging system allows detailed monitoring of heat generation, heat transfer, as well as the physiochemical transformation in the surrounding system resulting from heat delivery at the nanometer to micrometer scale. For example, localized phase transitions can be observed, such as ice melting via photothermally excited gold

nanospheres,<sup>13</sup> or liposome formation by NIR-excited gold nanoshells.<sup>14</sup> Thermal mapping in the vicinity of photothermally excited gold nanoparticles has been demonstrated using fluorescence polarization anisotropy of fluorescein surrounding gold nanorods.<sup>15</sup> Other fluorescence properties, such as fluorescence intensity,<sup>16,17</sup> lifetime,<sup>18</sup> or peak shift,<sup>19,20</sup> have been exploited to monitor the local temperature. Ratiometric measurements using temperature-sensitive fluorescent dyes have been demonstrated to eliminate concerns in intensity-based fluorescence measurements due to changes in laser power or concentration, and photobleaching effects.<sup>21,22</sup> Oliver et al. demonstrated the temperature-dependent emission peak shift of the calcium indicator dye Indo-1.<sup>23</sup> Due to its far spectral separation from the NIR excitation beam, Indo-1 was initially employed for the model thermal microscopy studies presented here. In the past few years, temperature-dependent optical properties have been discovered in colloidal semiconductor quantum dots (QDs). The fluorescence properties of QDs have been suggested as robust thermometric scales via temperature-dependent photoluminescence intensity changes or emission peak shifts,<sup>19,20,24–27</sup> leveraging the photostability and brightness of QDs in comparison to organic fluorophores, such as Indo-1. In order to develop temperature measurement techniques

**Received Date:** April 16, 2010

**Accepted Date:** May 7, 2010

**Published on Web Date:** May 19, 2010

using sensors including ratiometric organic dyes and colloidal QDs, common approaches involve such sensors dispersed in solution in which a group of gold nanoparticles is immobilized. However, in reality, NIR excitation often induces fluctuations in the physical states (e.g., clustering, dispersion, and thermophoresis) of gold nanoparticles. Therefore the interrelationship between the fluctuation of these physical properties and the ratiometric optical properties of these sensors is key to precise measurements assessing the local temperature change in the proximity of a group of nanoparticles. The unique advantage of image-based thermometry is the capability to directly visualize the physical states of gold nanoparticles during the photothermal energy conversion process while fluorescence ratiometric measurements are being performed simultaneously. This approach allows for the establishment of a more precise model system, taking into account the physiochemical changes in the group of nanoparticles. Here, we apply a ratiometric multimodal imaging method to measure local temperature based on the fluorescence emission peak shifts of Indo-1 or QDs and examine the dynamic motion of NIR-excited gold/silica nanoshells (silica core with an outer gold layer), chosen for their exceptionally large absorption cross section in the NIR regime.<sup>28</sup>

The spectral shifts of Indo-1 and QD sensors as a function of temperature were confirmed in cuvette measurements using a temperature-controlled PTI spectrofluorimeter in ranges of 20–50 °C for Indo-1 or 20 to 80 °C for QDs. As the temperature increases, the emission peak of Indo-1 blue shifts, while the QD peak red shifts. Separate microscopy calibration curves were generated for each sample, taking fluorescence ratios from room temperature (22 °C) through 40 °C in 5 °C increments. The temperature dependences of the peak ratios were approximated as linear throughout this temperature range.

To demonstrate the ability of the fluorophore to monitor photothermal temperature fluctuations, we monitored the emission shifts of Indo-1 fluorophores in solution as a function of the 785 nm radiation power focused upon a cluster of nanoshells. Nanoshells are packed into dense clusters by the preparation process of drying nanoshell solutions on the substrate, and many remain adhered to the surface after the coverglass surface is hydrated in a temperature-controlled aqueous fluid cell. Upon focusing the NIR to a small spot (20 μm diameter, 14 kW/cm<sup>2</sup>) on the nanoshell cluster, time-series images of the sample area with the nanoshell cluster were simultaneously collected in three different bandwidths: NIR range to image the focused NIR beam and two fluorescence bandwidths for ratiometric fluorescence imaging. Figure 1 displays a collection of single-frame images selected from the movies, from which the NIR power-dependent temperature fluctuation of the entire view-field area is determined by taking the ratio of the electron multiplying charge-coupled device (EM-CCD) background-corrected signals from the two Indo-1 emission channels. As the NIR radiation continues, the relative signal intensity measured from the 400–420 nm band (compared to the 490–510 nm band) increases. A temperature rise of ~2 K is observed throughout the image after NIR excitation, with noticeable spatial noise

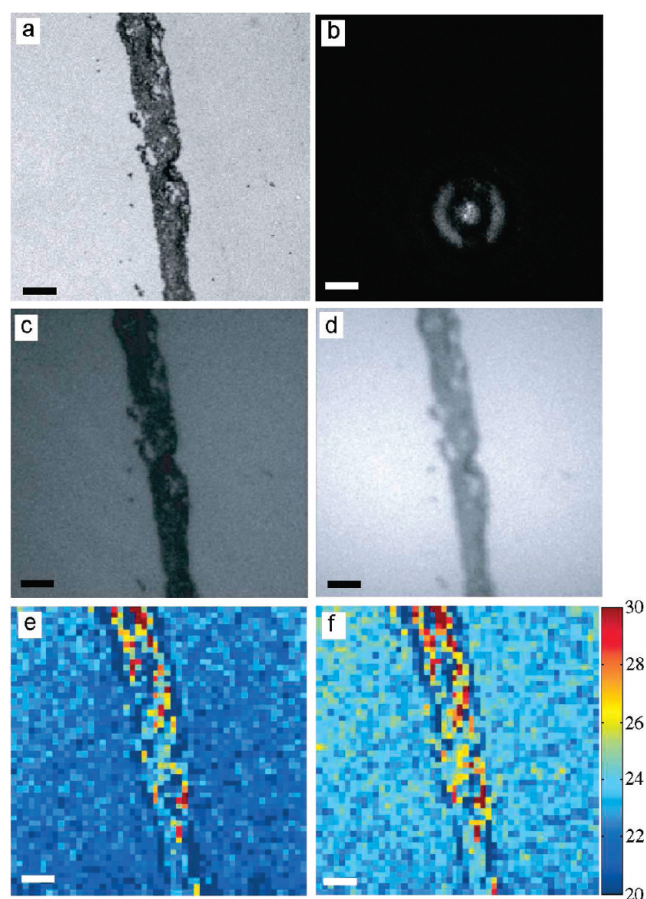


**Figure 1.** Multimodal imaging of a cluster of gold nanoshells. Sample is placed in a temperature-controlled liquid cell with fluorescent dye Indo-1. (a) Brightfield image of a nanoshell cluster. Nanoshells appear as dark spots. (b) The NIR beam is focused onto a small area on this cluster. The temperature can be recorded by monitoring the emission shift of Indo-1 deduced from the ratio of the emission bands in (c) 400–420 nm and (d) 490–510 nm, with example calculated temperature profiles (e) before and (f) during NIR excitation displayed with the color bar in °C. Scale bars are 20 μm.

primarily caused by the EM-CCD. Such noise can be reduced by spatial and/or temporal averaging or adjustment of the acquisition parameters (exposure time, excitation intensity, etc.). The change in mean temperature measured across the field of view as the shutter to the NIR beam is opened and closed is shown in Figure 2. During the 50 s heating time in each open-close cycle, the temperature change appears to reach the plateau, implying that thermal equilibrium is reached on the order of minutes. Experiments where the shutter is opened for 5 min demonstrate that the temperature reaches equilibrium within 90 s and that, regardless of the 785 nm radiation power, only minor variations exist in the heating profile across the field of view (Supporting Information, Figure S1). As an estimate of the error in the temperature measurement, the standard deviation of the mean  $\Delta T$  at equilibrium was determined to be ~0.05 K. It is also noteworthy that, when the 785 nm beam is blocked, the cooling process takes about the same time as the heating cycle, indicating that these heating/cooling cycles are primarily

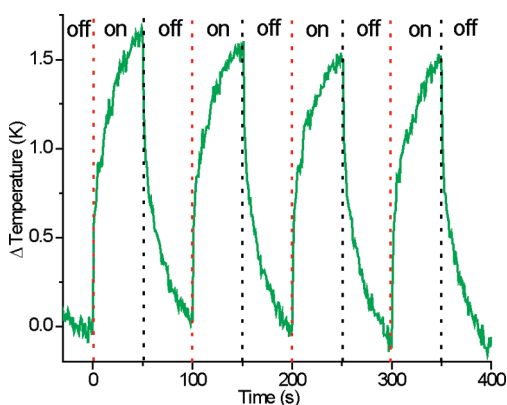


**Figure 2.** Temperature change as a function of time determined by analysis of the Indo-1 peak shift. The NIR excitation beam is initially blocked by a shutter. The shutter is opened and closed at 50 s intervals with corresponding heating and cooling cycles observed in the temperature trace.

based on thermal equilibrating processes between the nanoparticles and the bulk. These heating/cooling cycles are reproducible, and similar results were observed using QD emission shifts. Minimal heating occurs in the absence of nanoshells ( $\Delta T \approx 0.2$  K). In cases where nanoparticle concentrations are high, NIR heating can induce solvent evaporation, causing a bubble to appear in the excitation spot. The thermal gradients measured are much greater ( $\Delta T \approx 8$  K mean field of view) with elevated temperatures near the bubble ( $\Delta T > 50$  K – temperature must be extrapolated above microscopy calibration range). Figure S2 (Supporting Information) shows the temperature measurements obtained from a sample exhibiting bubble formation.

In addition to visualizing the changing thermal gradient, the motion of nanoparticles in the system can be monitored. Even small thermal gradients can induce fluid or particle motion, especially in confined thin films. Thermophoretic colloidal attraction has been reported previously and attributed to thermal gradient-induced slip-flow.<sup>29–31</sup> Confinement of small molecules using an optically driven thermal gradient and fluid flow has been demonstrated recently on thin films.<sup>32</sup> Specifically, localized heating of a substrate simultaneously caused thermophoresis of DNA and fluid flow perpendicular to the temperature gradient, resulting in focusing of the DNA. Although investigating a different system (direct heating of nanoparticles and thicker fluid layer), our multimodal imaging system visualizes similar focusing of the gold nanoshells within the focal volume of the excitation beam. Without NIR excitation, those nanoshells not in contact with the coverglass undergo Brownian motion. Upon photothermal excitation of a cluster of nanoshells, long-range directed motion of nanoshells in solution toward the excitation spot throughout the field of view ( $\sim 200 \mu\text{m}$ ) has been observed. Blocking the NIR beam or moving it to a nanoshell-free location halts this directed motion. The degree of motion is dependent on the excited nanoshell density and the power density of the NIR laser.

To determine whether the long-range nanoshell motion was caused by thermally-induced fluid flow or isothermal

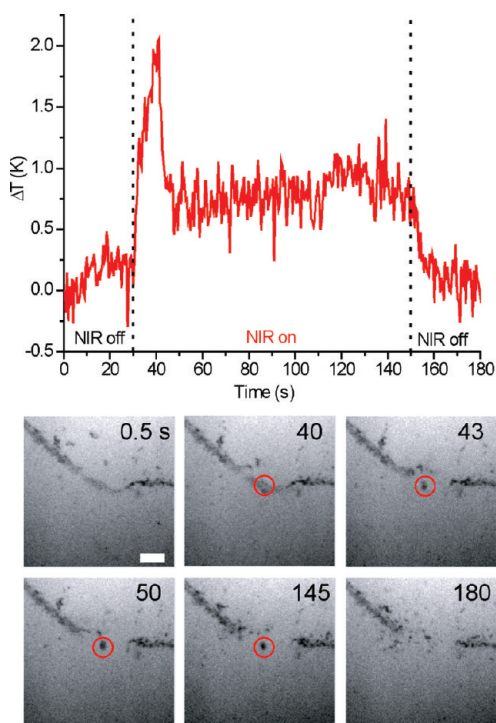


**Figure 3.** (Top) The temperature change recorded by the shift in the QD emission peak and (Bottom) selected images of the microscopic area under investigation (from 520 nm –550 nm signal). The presence of red circle indicates a NIR beam in this region. Photothermally excited nanoshells initially exhibit a high heat flux. This generates a fluid flow pulling several nearby nanoshells toward the excitation spot, and these form a highly dynamic “cloud.” The temperature shift diminishes as a result of decreased numbers of nanoshells in the focused spot (many nanoshells have detached from the coverglass). Once the NIR beam is blocked, the nanoparticles return to Brownian motion, and the cloud dissipates. Scale bar is 20  $\mu\text{m}$ , and all images are at the same magnification.

optical trapping by the focused NIR light, we imaged a sample containing polystyrene fluorescent microbeads (FluoSpheres, 0.2  $\mu\text{m}$ , Invitrogen) as indicators of the flow of the aqueous medium. When nanoshells are absent or present without NIR excitation, the beads exhibit only Brownian motion. Under tightly focused NIR irradiation, some beads become trapped at the excitation spot, possibly via purely optical phenomenon (i.e., optical tweezers effect resulting from optical gradient forces).<sup>35</sup> However, when the sample contains NIR-excited nanoshells, large directed movement of beads are observed (across the entire view field). Beads close to the coverglass surface are observed to move quickly toward to the NIR focus, and a “hole” lacking beads forms at the excitation center (as beads move perpendicularly away from the surface and out of the focal plane). Beads 200  $\mu\text{m}$  above the surface are observed moving away from the NIR excitation beam. These results suggest that the thermally induced bidirectional convective fluid flow observed by Weinert and Braun<sup>32</sup> may also exist in our system.

This particle focusing phenomenon must be considered when monitoring the temperature changes induced by photothermally excited nanoparticles. Several important scenarios

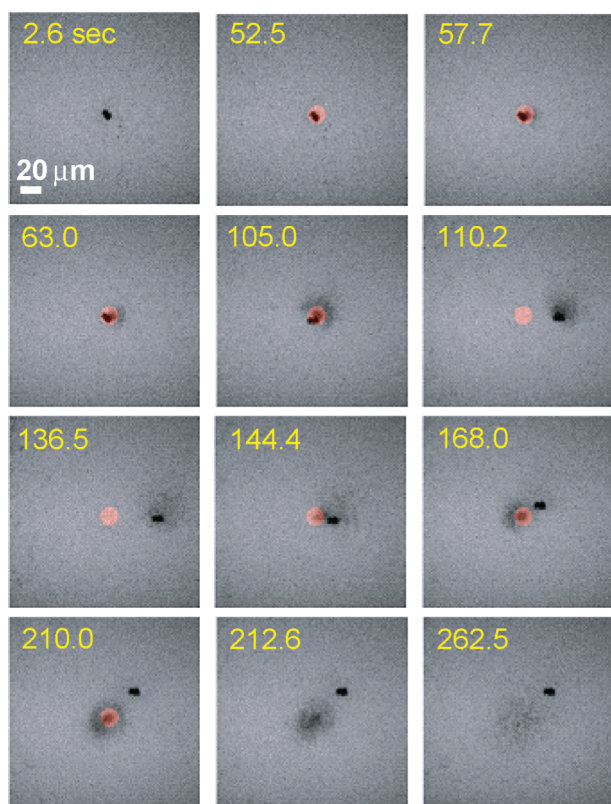


**Figure 4.** Focusing of nanoshells during photothermal NIR excitation (indicated by red spot) occurs when sufficient nanoshells are present. A nanoshell cluster (black) is initially heated. Nanoparticles ejected from this cluster during excitation, as well as particles farther away in solution are pulled toward the excitation spot. If the excitation beam moves away quickly (by moving the sample stage), nanoparticles do not follow, nor do other particles move to the new beam location. However, moving the beam slowly allows the cloud of nanoparticles to be dragged. Nanoparticles diffuse freely once excitation is halted. The image is generated by the 490–510 nm emission band of Indo-1. All images are at the same magnification.

have been observed. Fluid motion can cause sudden dispersal of nanoshell aggregates lowering the temperature change, or can focus nanoshells into a small region thereby enhancing system heating. An example of focusing and subsequent dispersal of nanoshells along with the recorded temperature change is displayed in Figure 3. The nanoshells begin in a large clustered line prior to laser excitation. Shortly after NIR excitation commences, many of the nanoshells move from the coverglass surface as they are pulled by the fluid flow toward the excitation spot. An initial temperature rise occurs upon NIR excitation, but heat generation decreases as the number of nanoshells in the focal area has diminished due to the fluid motion, despite the focusing of some of those nanoparticles into a dense “cloud.” Such motion complicates the determination of appropriate excitation powers with dosimetry measurements. This behavior can be mitigated by use of lower laser power densities (due to smaller thermal gradients). Indeed, a region of similar nanoshell density as that shown in Figure 3 was exposed to a diffuse NIR beam, resulting in an equilibrium mean temperature elevation of  $\sim 1$  K.

Aside from focusing nanoshells into a small area using the thermal gradient, nanoshells can be repositioned using this methodology. If the NIR beam is moved slowly, the nanoshell cloud can be dragged through the solution (Figure 4). If the excitation beam moves away quickly, nanoparticles do not follow, nor do other particles move to the new location. However, moving the beam slowly allows the cloud of nanoparticles to be dragged. Nanoparticles diffuse freely once excitation is halted. Dynamic fluid motion induced by particle heating is noteworthy for its potential to dramatically increase the induced temperature rise due to particle focusing balanced against the temperature losses induced through increased convection. Selection of appropriate laser power densities and nanoparticle concentrations should be informed by this behavior, as well as the potential to create microbubbles under high laser power and dense nanoparticle clusters. While heat generated in from the nanoparticles dissipates rapidly, the nanoparticles and the surrounding nanoscale environment will experience elevated temperature differentials compared to the surrounding media.

The multimodality imaging method presented here is not limited to gold nanoshells. The photothermal excitation beam can be adjusted to suit the nanoparticles under investigation (e.g., in the visible region for gold nanospheres), and different temperature sensitive fluorophores can be chosen to optimize the separation between the excitation beams and the emission signals. These imaging techniques allow both profiling and control of the photothermal excitation beam as well as monitoring of the heat transfer from the nanoparticles to their surroundings. This method can be readily expanded to 3D imaging by combining z-slices from different focal planes. Especially if combined with other thermal imaging modalities that probe nanoscale heating, such as single particle heterodyne imaging and bulk IR thermometry, a detailed multiscale model of the heat transfer into the surrounding system can be developed with implications for the development of nanotherapeutics and device construction.

## EXPERIMENTAL METHODS

Clusters of nanoshells (60 nm silica core and 20 nm gold coating layer; absorption maximum near 785 nm) were formed by pipetting 10  $\mu$ L of nanoshell solution ( $5.65 \times 10^9$  nanoparticles/mL) onto a 40 mm coverglass and allowing the solution to dry. This sample is then placed in a temperature-controlled Biotech (Butler, PA) FCS2 fluid cell using a 0.5 mm thick gasket with a solution containing 0.08  $\mu$ mol/L QDs (525 nm emission, carboxylated, Invitrogen, Carlsbad, CA) or 6  $\mu$ mol/L Indo-1 (Invitrogen). Large clusters of the nanoshells remain adsorbed to the glass, with freely diffusing nanoshells also present.

We modified an Olympus IX-81 inverted microscope (Olympus America, Center Valley, PA) to allow multimodal imaging using simultaneous NIR excitation of the nanoshells, UV excitation of Indo-1 (or 457 nm Ar laser excitation of QDs), and bright-field imaging of the sample. A 750 nm short pass filter was placed at a 45° angle above the bright-field condenser. This reflected a beam from a continuous wave 785 nm laser diode (Thorlabs, Newton, NJ) through the 0.55 NA

condenser focusing the beam onto the sample. Light from the tungsten lamp can pass through the short pass filter for bright-field illumination. The 785 nm diode laser power is adjusted via LabVIEW (National Instruments, Austin, TX). Experiments presented here used a power of 45 mW after the condenser. Light from a mercury burner was filtered through a 350/50 nm bandpass to provide UV excitation. The sample was imaged through a 20x UMPlanFl 0.46 NA objective (Olympus). Optical signals were filtered by a 416/501 bandpass filter for Indo-1 emission (Semrock, Rochester, NY) and a 550 nm short-pass filter and imaged onto an EM-CCD camera (Andor Technology, Ireland). For multimodal imaging, the signal was split according to wavelength and imaged onto quadrants of the EM-CCD using a Quad-View multimodal imager (Photometrics, Tuscon, AZ) with D405/30 M and D485/25 M filters for the low and high wavelength portions of the Indo-1 peak. Signals from the QDs were passed through 510DF15 and HQ535/30 filters. Ratio-metric image analysis was performed in MATLAB (Mathworks, Natick, MA). Background drift was corrected by fitting the initial and end points of the data set.

**SUPPORTING INFORMATION AVAILABLE** Additional figures as mentioned in the text and videos of nanoparticle focusing. This material is available free of charge via the Internet at <http://pubs.acs.org>.

#### AUTHOR INFORMATION

##### Corresponding Author:

\*To whom correspondence should be addressed. E-mail: [jch@nist.gov](mailto:jch@nist.gov). Phone: 301-975-4580. Address: National Institute of Standards and Technology, 100 Bureau Drive, Mailstop 8443, Gaithersburg, MD 20899.

**ACKNOWLEDGMENT** The authors thank Naomi Halas at Rice University for the donation of the gold nanoshells. Additionally, we thank Rani Kishore, Brooke Hester, Kris Helmersen, and HyeongGon Kang at NIST and Zhuomin Zhang, David Citrin, and Nazli Donmez of Georgia Institute of Technology for helpful discussions. S.G.C. was supported and M.L.C. was partially supported by a National Research Council Fellowship. J.H. was supported by the NIST Innovation in Measurement Science Program. Certain commercial equipment, instruments, or materials are identified in this paper to foster understanding and does not imply recommendation or endorsement by NIST, nor does it imply that the materials or equipment identified are necessarily the best available for the purpose.

#### REFERENCES

- (1) Tong, L.; Zhao, Y.; Huff, T. B.; Hansen, M. N.; Wei, A.; Cheng, J. X. Gold Nanorods Mediate Tumor Cell Death by Compromising Membrane Integrity. *Adv. Mater.* **2007**, *19*, 3136–3141.
- (2) Hirsch, L. R.; Stafford, R. J.; Bankson, J. A.; Sershen, S. R.; Rivera, B.; Price, R. E.; Hazle, J. D.; Halas, N. J.; West, J. L. Nanoshell-Mediated Near-Infrared Thermal Therapy of Tumors under Magnetic Resonance Guidance. *Proc. Natl. Acad. Sci. U.S.A.* **2003**, *100*, 13549–13554.
- (3) Chen, J. Y.; Wang, D. L.; Xi, J. F.; Au, L.; Siekkinen, A.; Warsen, A.; Li, Z. Y.; Zhang, H.; Xia, Y. N.; Li, X. D. Immuno Gold Nanocages with Tailored Optical Properties for Targeted Photothermal Destruction of Cancer Cells. *Nano Lett.* **2007**, *7*, 1318–1322.
- (4) Pissuwan, D.; Valenzuela, S. M.; Cortie, M. B. Therapeutic Possibilities of Plasmonically Heated Gold Nanoparticles. *Trends Biotechnol.* **2006**, *24*, 62–67.
- (5) Pitsillides, C. M.; Joe, E. K.; Wei, X. B.; Anderson, R. R.; Lin, C. P. Selective Cell Targeting with Light-Absorbing Microparticles and Nanoparticles. *Biophys. J.* **2003**, *84*, 4023–4032.
- (6) Zharov, V. P.; Mercer, K. E.; Galitovskaya, E. N.; Smeltzer, M. S. Photothermal Nanotherapeutics and Nanodiagnostics for Selective Killing of Bacteria Targeted with Gold Nanoparticles. *Biophys. J.* **2006**, *90*, 619–627.
- (7) Hodak, J. H.; Martini, I.; Hartland, G. V. Spectroscopy and Dynamics of Nanometer-Sized Noble Metal Particles. *J. Phys. Chem. B* **1998**, *102*, 6958–6967.
- (8) Averitt, R. D.; Westcott, S. L.; Halas, N. J. Ultrafast Electron Dynamics in Gold Nanoshells. *Phys. Rev. B* **1998**, *58*, R10203–R10206.
- (9) Hu, M.; Hartland, G. V. Heat Dissipation for Au Particles in Aqueous Solution: Relaxation Time versus Size. *J. Phys. Chem. B* **2002**, *106*, 7029–7033.
- (10) Harris, N.; Ford, M. J.; Cortie, M. B. Optimization of Plasmonic Heating by Gold Nanospheres and Nanoshells. *J. Phys. Chem. B* **2006**, *110*, 10701–10707.
- (11) Roper, D. K.; Ahn, W.; Hoepfner, M. Microscale Heat Transfer Transduced by Surface Plasmon Resonant Gold Nanoparticles. *J. Phys. Chem. C* **2007**, *111*, 3636–3641.
- (12) Seol, Y.; Carpenter, A. E.; Perkins, T. T. Gold Nanoparticles: Enhanced Optical Trapping and Sensitivity Coupled with Significant Heating. *Opt. Lett.* **2006**, *31*, 2429–2431.
- (13) Richardson, H. H.; Hickman, Z. N.; Govorov, A. O.; Thomas, A. C.; Zhang, W.; Kordesch, M. E. Thermo-optical Properties of Gold Nanoparticles Embedded in Ice: Characterization of Heat Generation and Melting. *Nano Lett.* **2006**, *6*, 783–788.
- (14) Clarke, M. L.; Kang, H.-G.; Yim, P. B.; Kishore, R.; Helmersen, K.; Hwang, J. Thermal Properties of Gold Nanoshells in Lipid Vesicles Studied by Single Particle Tracking Measurements. *Proc. SPIE* **2008**, *6849*, 68490H.
- (15) Baffou, G.; Kreuzer, M. P.; Kulzer, F.; Quidant, R. Temperature Mapping near Plasmonic Nanostructures Using Fluorescence Polarization Anisotropy. *Opt. Express* **2009**, *17*, 3291–3298.
- (16) Ross, D.; Gaitan, M.; Locascio, L. E. Temperature Measurement in Microfluidic Systems Using a Temperature-Dependent Fluorescent Dye. *Anal. Chem.* **2001**, *73*, 4117–4123.
- (17) Khalil, G. E.; Lau, K.; Phelan, G. D.; Carlson, B.; Gouterman, M.; Callis, J. B.; Dalton, L. R. Europium Beta-Diketonate Temperature Sensors: Effects of Ligands, Matrix, and Concentration. *Rev. Sci. Instrum.* **2004**, *75*, 192–206.
- (18) Benninger, R. K. P.; Koc, Y.; Hofmann, O.; Requejo-Isidro, J.; Neil, M. A. A.; French, P. M. W.; deMello, A. J. Quantitative 3D Mapping of Fluidic Temperatures within Microchannel Networks Using Fluorescence Lifetime Imaging. *Anal. Chem.* **2006**, *78*, 2272–2278.
- (19) Li, S.; Zhang, K.; Yang, J. M.; Lin, L. W.; Yang, H. Single Quantum Dots as Local Temperature Markers. *Nano Lett.* **2007**, *7*, 3102–3105.
- (20) Han, B.; Hanson, W. L.; Bensalah, K.; Tuncel, A.; Stern, J. M.; Caddeu, J. A. Development of Quantum Dot-Mediated Fluorescence Thermometry for Thermal Therapies. *Ann. Biomed. Eng.* **2009**, *37*, 1230–1239.
- (21) Sakakibara, J.; Adrian, R. J. Whole Field Measurement of Temperature in Water Using Two-Color Laser Induced Fluorescence. *Exp. Fluids* **1999**, *26*, 7–15.

- (22) Ebert, S.; Travis, K.; Lincoln, B.; Guck, J. Fluorescence Ratio Thermometry in a Microfluidic Dual-Beam Laser Trap. *Opt. Express* **2007**, *15*, 15493–15499.
- (23) Oliver, A. E.; Baker, G. A.; Fugate, R. D.; Tablin, F.; Crowe, J. H. Effects of Temperature on Calcium-Sensitive Fluorescent Probes. *Biophys. J.* **2000**, *78*, 2116–2126.
- (24) Wang, S. P.; Westcott, S.; Chen, W. Nanoparticle Luminescence Thermometry. *J. Phys. Chem. B* **2002**, *106*, 11203–11209.
- (25) Walker, G. W.; Sundar, V. C.; Rudzinski, C. M.; Wun, A. W.; Bawendi, M. G.; Nocera, D. G. Quantum-Dot Optical Temperature Probes. *Appl. Phys. Lett.* **2003**, *83*, 3555–3557.
- (26) Turyanska, L.; Patane, A.; Henini, M.; Hennequin, B.; Thomas, N. R. Temperature Dependence of the Photoluminescence Emission from Thiol-Capped PbS Quantum Dots. *Appl. Phys. Lett.* **2007**, *90*, 101913.
- (27) Jing, P. T.; Zheng, J. J.; Ikezawa, M.; Liu, X. Y.; Lv, S. Z.; Kong, X. G.; Zhao, J. L.; Masumoto, Y. Temperature-Dependent Photoluminescence of CdSe-Core CdS/CdZnS/ZnS-Multishell Quantum Dots. *J. Phys. Chem. C* **2009**, *113*, 13545–13550.
- (28) Cole, J. R.; Mirin, N. A.; Knight, M. W.; Goodrich, G. P.; Halas, N. J. Photothermal Efficiencies of Nanoshells and Nanorods for Clinical Therapeutic Applications. *J. Phys. Chem. C* **2009**, *113*, 12090–12094.
- (29) Duhr, S.; Braun, D. Why Molecules Move Along a Temperature Gradient. *Proc. Natl. Acad. Sci. U.S.A.* **2006**, *103*, 19678–19682.
- (30) Weinert, F. M.; Braun, D. Observation of Slip Flow in Thermophoresis. *Phys. Rev. Lett.* **2008**, *101*, 168301.
- (31) Di Leonardo, R.; Ianni, F.; Ruocco, G. Colloidal Attraction Induced by a Temperature Gradient. *Langmuir* **2009**, *25*, 4247–4250.
- (32) Weinert, F. M.; Braun, D. An Optical Conveyor for Molecules. *Nano Lett.* **2009**, *9*, 4264–4267.
- (33) Ashkin, A.; Dziedzic, J. M.; Bjorkholm, J. E.; Chu, S. Observation of a Single-Beam Gradient Force Optical Trap for Dielectric Particles. *Opt. Lett.* **1986**, *11*, 288–290.